NASA-CR-197534

NAG-1636

THE MASS AND DYNAMICS OF cD CLUSTERS WITH COOLING FLOWS.
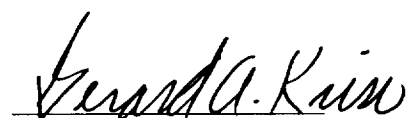## I. ROSAT OBSERVATIONS OF A 496

Gerard A. Kriss

Department of Physics & Astronomy, Johns Hopkins University, Baltimore, MD 21218

Abstract

As part of a program to determine the mass distribution of cD galaxy clusters with cooling flows, we obtained a ROSAT image of the cluster A 496. The image reveals sharply peaked emission centered on the cD galaxy. Both the peaked cooling flow emission and the more extended emission filling the cluster are centered on the cD galaxy to within $15''$. The surface brightness profile is consistent with previous *Einstein* observations. We measure spatially resolved spectra for the X-ray emission, and find a significant decline in temperature in the innermost $2'$ to $4'$. We also find a gradient in absorption due to cold neutral gas, with an excess above the neutral hydrogen column due to our own galaxy in the inner $4'$. The excess absorption, however, is far below previously reported values. The surface brightness profile and the spatially resolved temperature profile are indicative of a cooling flow in this cluster. Cooling flow models fit to the X-ray spectra in the innermost $2'$ yield a mass flow rate of 59 $M_{\odot}$ yr^{-1}.

The spatially resolved temperature and surface brightness profiles are used to derive the mass distribution of the cluster both in the hot, X-ray emitting plasma and in the unseen dark matter that binds the cluster. To a radius of 1.0 Mpc we find a total cluster mass of 3.44×10^{14} $M_{\odot}$; the X-ray emitting gas mass of 0.75×10^{14} $M_{\odot}$ to this radius comprises 16% of the total cluster mass.

Gerard A. Kriss
Principle Investigator
December 15, 1994

1. Introduction

The rich cluster of galaxies A 496 (Abell 1958) is one of the brightest X-ray clusters. It is relatively nearby ($z = 0.033$; Malumuth et al. 1992), making it easy to study at both optical and X-ray wavelengths. Malumuth et al. 1992 have obtained over 140 redshifts for individual galaxies in the cluster, and they find the distribution to be smooth and regular with little evidence for sub-structure. Like the optical structure of the cluster, the X-ray structure is also relatively simple. The surface brightness distribution is sharply peaked on the central cD galaxy, and low-energy X-ray spectra obtained with the Solid State Spectrometer (SSS) on the *Einstein Observatory* show cool gas with spectral lines indicative of a strong cooling flow (Nulsen et al. 1982). Subsequent re-analysis of these same data (White et al. 1992) show that in addition to the low central temperature, there appears to be excess absorption by cold gas, which they infer to be cold material condensing from the cooling flow.

As a dynamically simple system, A 496 is thus an ideal laboratory for comparing optical and X-ray determined measures of the cluster mass distribution. If these agree to first order, one could envision using the ultimately more reliable X-ray mass distribution as a constraint for then studying the dynamics of the galaxy orbits in the cluster. To probe the X-ray structure of the cluster more deeply and to obtain spatially resolved temperature profiles of A 496 we performed X-ray observations using ROSAT.

2. Observations and Data Reduction

Our ROSAT position-sensitive proportional counter (PSPC) image of A 496 was obtained on 1991 March 6. The image was centered on the cD galaxy at $\alpha_{2000} = 4^h33^m38\overset{s}{.}4$, $\delta_{2000} = -13°15'36\overset{''}{.}0$. In the delivered data products three separate observation intervals were summed to create the final image representing 8972 s of live observing time. The spacecraft wobble was normal, and there do not appear to be any extraordinary problems associated with the observation or the subsequent processing of the data.

Since the cluster emission in A 496 covers a significant fraction of the field in our observation, we have used S. L. Snowden's extended source analysis package to re-extract the data and to form background-subtracted, vignetting-corrected images (cf. Snowden et al. 1994). Including in our final image only those data intervals for which the Master Veto (MV) rate was less than 170 cts s^{-1}, our final image contains 7256 s of valid data. Non-cosmic detector background was subtracted as described by Snowden et al. (1992)

and Plucinsky et al. (1993). The resulting image was corrected for vignetting using the exposure maps generated by the extended source analysis package.

3. Data Analysis

In the subsequent analysis the background is assumed to be spatially invariant. For computing our surface brightness profile, we use a background determined from regions free of supporting rib shadows at radii from $40'$ to $60'$. For our spectral analysis, we use the annulus from $24'$ to $44'$ to establish the background surface brightness and its spectrum. We assume a Hubble constant of $H_o = 50$ km s^{-1} Mpc^{-1} and a deceleration parameter $q_o = 0$ throughout.

3.1. Spatial Structure

The extended X-ray emission from A 496 and its centrally peaked surface brightness are apparent in the contour plot shown in Figure 1. The vignetting-corrected data have been binned into $15''$ pixels for this display.

To test whether the peaked emission centered on the cD galaxy might be physically distinct from the more diffuse cluster-filling emission, we fit the image with a composite model consisting of an ellipsoidal surface brightness distribution plus a Gaussian point source of dispersion $25''$. This gives a good fit to the observed image. It is clearly ellipsoidal with the major axis at a position angle of $112°$ and an ellipticity $1 - b/a = 0.14$. Within the errors, however, the point source is centered at the same location as the more extended cluster emission.

Ignoring the slight ellipticity revealed by this analysis, we extract an azimuthally averaged surface brightness profile which is shown in Figure 2. To empirically characterize the spatial distribution of the X-ray emission, we describe the surface brightness profile with an isothermal "β" model:

$$I_x(r) = I_{x0}[1 + (\frac{r}{r_c})^2]^{-3\beta + 1/2} \tag{1}$$

where I_{x0} is the central surface brightness and r_c is the core radius. β is defined as

$$\beta \equiv \frac{\mu m_p \sigma_r^2}{kT_g},$$

where μ is the mean molecular weight in amu, m_p is the mass of the proton, σ_r is the line-of-sight velocity dispersion of the galaxies in the cluster, and T_g is the temperature of the gas.

The relatively sharp peak centered on the cD galaxy in our image results in a very poor fit to this model surface brightness profile. The central peak is resolved, however, and so we have chosen to characterize it with a second β–model component. This choice is qualitatively justified by the presence of two clear inflection points in the surface brightness profile shown in Figure 2. Physically, one could interpret this as X-ray emission from the cluster as a whole with gas trapped in the potential well of the central cD galaxy providing the second component. In practice to perform the actual fits we describe the X-ray emission using the sum of two spherically symmetric volume emissivity profiles which individually project onto the sky as β models:

$$E_{x,tot}(r) = E_{x1}[1 + (\frac{r}{r_{c1}})^2]^{-3\beta_1} + E_{x2}[1 + (\frac{r}{r_{c2}})^2]^{-3\beta_2} \qquad (2)$$

The subscript 1 indicates values for the central galaxy potential well and subscript 2 indicates values associated with the cluster potential well. The volume emissivity is numerically projected onto the sky and then convolved with the PSPC point response function, which is assumed to be a Gaussian of dispersion 10.5 arcsec. The fit has a total of six free parameters: E_{x1}, E_{x2}, r_{c1}, r_{c2}, β_1 and β_2. Background was used as a free parameter initially and then fixed before final fits were made. Because of uncertainties in the background, data taken beyond 21 arcmin are not used in the fits. Best-fit values for the parameters are given in Table 1. The core radius of 240 kpc for the cluster-filling component of the hot gas compares favorably with the value of 225 kpc previously obtained by Abramopoulos & Ku (1983) using *Einstein* IPC data. (Their fits assumed a value for β fixed at 1.0.)

3.2. Spectra

Again ignoring the ellipticity, we extracted spatially resolved spectra from the image in circular annuli centered on the peak of the surface brightness distribution. Annuli were chosen so that the total number of counts in each one was equal. We fit the extracted spectra with single-temperature Raymond & Smith (1977) thermal models using the xspectral package in PROS. In our fits the temperature (T), the column density of neutral hydrogen absorption (N_H), the abundance of the emitting gas, and the overall normalization of the spectrum are permitted to vary freely. Our fits are restricted to energy channels 6–34

spanning the energy range 0.20–2.48 keV. Data at the lowest energies are excluded to avoid uncertainties in the PSPC response matrix. We use the latest calibration files as distributed with the release of PROS 2.3 in 1993 December. All annuli produce satisfactory fits which are summarized in Table 2.

The spatially resolved spectra we have obtained of A 496 show both a clear temperature gradient associated with the cooling flow, and evidence for excess absorption by cold gas in the same spatial region. The temperature profile illustrated in Figure 3 shows a distinct drop in the innermost annulus. The absorption by cold gas is in excess of the galactic value of $\sim 4.3 \times 10^{20}$ cm^{-2} (Stark et al. 1992) within the central $6''\!.25$. The apparent deficit at large radius is within the systematic errors introduced by our choice of background. Changes of 1% in the normalization of the background spectrum can change the best-fit value for log N_H in this outermost annulus by 0.1.

Given the poor fit in the central region and the evidence for a cooling flow, we have fit the spectrum of the central 2′ with a cooling flow model. This model is decsribed by Mushotzky & Szymkowiak (1988), and it assumes gas cools at a constant mass flow rate from the upper temperature of the general intracluster medium to a lower temperature. Parcels of gas at intermediate temperatures have relative emission measures described by a power law—EM $\sim$ (T/T$_{high}$)$^{\alpha_{EM}}$. Free parameters in the fit are T$_{low}$, the column density of neutral gas absorption local to the cluster (foreground galactic absorption is fixed at $N_H = 4.3 \times 10^{20}$ cm^{-2}), the mass flow rate, $\dot{M}$, and the power law index of the emission measure distribution, α_{EM}. This model gives a significantly better fit to the central spectrum as summarized in Table 3. The mass flow rate of 59 $M_\odot$ yr^{-1} is also in reasonable agreement with that obtained by White et al. 1992 (65^{+29}_{-23} $M_\odot$ yr^{-1}).

4. Discussion

The temperature of 2.77 keV in the innermost 2′ is consistent with the SSS observations which show a mixture of cold gas at ~ 1.4 keV and hotter gas at ~ 6 keV (Nulsen et al. 1982). The temperatures at larger radii all match the globally averaged higher temperature of $4.8^{+1.0}_{-0.8}$ keV as seen with the medium energy proportional counters on EXOSAT (Edge & Stewart 1991). The abundance of approximately half solar is typical of rich clusters, and also matches the Fe abundance as measured with EXOSAT.

Our evidence for excess absorption by cold gas in the same spatial region as the cooling flow bolsters arguments that this is material condensing out of the cooling flow (White et al. 1992). While we do see excess absorption of $\sim 1.2 \times 10^{20}$ cm^{-2} above galactic, this is more than an order of magnitude lower than the value of $\sim 2.0 \times 10^{21}$ cm^{-2} reported by White et

al. (1991). Absorption at $\sim 2.0 \times 10^{21}$ cm^{-2} can be excluded at high confidence. The reason for the discrepancy is not clear. While uncertainties in the background subtraction may have some effect on our fits at the larger radii, the background correction in the innermost $2'$ is almost negligible. The cooling flow model fit to our data also shows evidence for excess absorption by cold gas, but again the excess absorption is an order of magnitude lower than that found by White et al. 1992. Given that cool gas produces substantial amounts of line emission that is not resolved in the PSPC and is partly resolved by the SSS, it is possible that the PSPC is simply not as sensitive to the mix of high temperature and low temperature gas that leads to the SSS results. ASCA observations should help to resolve this issue.

While the central cooling flow is intrinsically interesting, its influence on the overall properties of the cluster is limited to the very central regions. Beyond the central 100–200 kpc our data are consistent with a relatively isothermal temperature distribution which makes the determination of the gas density and the cluster mass profile rather straightforward. By folding the photon emissivity of the cluster gas through the response of the PSPC, we can directly relate our fitted emissivity for the cluster surface brightness to the density of the X-ray emitting gas—

$$C(n, T) = \frac{n^2}{4\pi D^2} \int \frac{\epsilon(E, T)}{E} A E e^{-N_H \sigma(E)} \, dE. \tag{3}$$

Here, n is the total particle density, $n^2 \epsilon(E, T)/E$ gives the photon emissivity of the gas, $A(E)$ is the effective area of the PSPC, and N_H is the galactic neutral hydrogen density. $\sigma(E)$ is the total cross section to X-ray absorption, which is calculated using the cross sections and abundances of Morrison & McCammon (1983).

The derived density profile for the hot gas is shown in Figure 5. Since the hot gas cools radiatively, the cooling time for a given parcel of gas is

$$t_{cool} = \frac{3/2 nkT}{n_e n_H \Lambda(T)} = \frac{3.33 \times 10^{10} \text{yr}(T/1\text{keV})}{(n/10^{-3} \text{ cm}^{-3})(\Lambda/10^{-23})} \tag{4}$$

where n^2 is the total particle density and $\Lambda(T)$ is the cooling function as given by Raymond et al. 1976. Using our temperature and density profiles we find that only gas interior to 55 kpc has a cooling time shorter than the Hubble time. Assuming that the gas at larger radii is isothermal and in hydrostatic equilibrium, the mass distribution required to bind the gas to the cluster follows directly as

$$M(< R) = \frac{-kTR}{G\mu m_p}\left(\frac{d\ln n}{d\ln R}\right). \tag{5}$$

This binding mass distribution is shown in Figure 6. The mass of the hot gas obtained by integrating the derived density profile is also shown. At the largest radius (1 Mpc) for which we have reliable measurements the cluster has a total mass of 3.44×10^{14} $M_{\odot}$. The hot gas to this radius has a cumulative mass of $0.75 \times 10^{14} M_{\odot}$, or 16% of the total.

It is insightful to compare our X-ray analysis with the extensive optical kinematical data of Malumuth et al. 1992. They find a line-of-sight velocity dispersion for the cluster of 700 km s^{-1}. For a mean cluster temperature of kT = 4.8 keV, the implied β is 0.61, which compares surprisingly well with the β of 0.62 measured using our surface brightness profile. For the 94 member galaxies within 1 Mpc of the cluster center, Malumuth et al. 1992 find masses ranging from $3.3 - 4.9 \times 10^{14}$ $M_{\odot}$, also in good agreement with our X-ray determinations.

In fact, since the optical and the X-ray measurements agree so closely, this implies that the galaxy orbit distribution must be close to isotropic, since the principle uncertainty in the optical mass determinations is the velocity dispersion tensor. The smooth, regular X-ray surface brightness profile, the lack of optical substructure in either the galaxy positions or their velocities, and this nearly isotropic orbit distribution all suggest that A 496 is well relaxed dynamically. In a future paper we will use the measured X-ray mass distribution with the projected galaxy velocity dispersion profile to set rigorous constraints on the allowed radial variations in the velocity dispersion tensor.

Table 1: β–Model Best Fit Values for A 496

Parameter	Value	90% Confidence Range
E_{x1} (10^{-7} cts s^{-1} arcsec^{-3})	43.91	43.10–44.70
r_{c1} (arcsec)	23.96	23.79–24.12
r_{c1} (kpc)	0.0218	0.0217–0.0220
β_1	0.519	0.517–0.521
E_{x2} (10^{-7} cts s^{-1} arcsec^{-3})	0.1580	0.1540–0.1620
r_{c2} (arcsec)	229.9	227.9–231.9
r_{c2} (kpc)	0.2098	0.2076–0.2119
β_2	0.618	0.613–0.622
Background (10^{-7} cts s^{-1} arcsec^{-3})	3.407	3.250–3.493
χ^2	33.97	
Degrees of Freedom	22	

Table 2: Raymond & Smith Thermal Spectra Fit to A 496.

Annulus (arc min)	kT (keV)	log N_H	Abundance	χ^{2a}
0–2	$2.77^{+0.43}_{-0.57}$	$20.70^{+0.03}_{-0.03}$	$0.75^{+1.25}_{-0.25}$	38.65
2–4	$4.28^{+2.82}_{-1.38}$	$20.78^{+0.03}_{-0.02}$	$0.75^{+3.25}_{-0.65}$	25.49
4–6.25	$4.81^{+\infty}_{-1.81}$	$20.76^{+0.04}_{-0.04}$	$0.75^{+4.25}_{-0.65}$	16.86
6.25–10	$4.77^{+\infty}_{-1.77}$	$20.62^{+0.06}_{-0.06}$	$0.75^{+4.25}_{-0.65}$	31.97
10–18	$2.95^{+2.25}_{-0.95}$	$20.45^{+0.09}_{-0.08}$	$0.75^{+2.25}_{-0.65}$	23.52

[a]Each tabulated fit includes 29 data points and 4 free parameters for a total of 25 degrees of freedom.

Table 3: Cooling Flow Spectrum Fit to A 496.

Annulus (arc min)	kT_{low} (keV)	kT_{high}[a] (keV)	$\log N_H$[b] (cm^{-2})	$\dot{M}$ ($M_\odot$ yr^{-1})	α_{EM}	Abundance	χ^2[c]
0–2	0.99	4.8	20.25	59	2.12	0.90	34.56

[a]The high temperature is fixed at the mean intracluster value.

[b]Foreground cold absorption is also included at the fixed galactic value of 4.3×10^{20} cm^{-2}.

[c]The fit includes 29 data points and 5 free parameters for a total of 24 degrees of freedom.

REFERENCES

Abell, G. O. 1958, ApJS, 3, 211

Edge, A. C., & Stewart, G.C. 1991, MNRAS, 252, 414

Malumuth, E. M., Kriss, G. A., Ferguson, H. C., Dixon, W. V. D., & Ritchie, C. 1992, AJ, 104, 495

Morrison, J., & McCammon, R., 1983, *Astrophys. J.*, **270**, 119

Mushotzky, R. F., & Szymkowiac, A. E. 1988, In "Cooling Flows in Clusters of Galaxies", ed. A. C. Fabian, Kluwer Academic Publishers, 53

Nulsen, P. E. J., Stewart, G. C., Fabian, A. C., Mushotzky, R. F., Holt, S. S., Ku, W. H.-M., & Malin, D. F. 1982, MNRAS, 199, 1089

Plucinsky, P., Snowden, S., Briel, U., Hasinger, G., & Pfefferman, E. 1993, ApJ, 999, 999

Raymond, J. C., & Smith, B. W. 1977, ApJS, 35, 419

Raymond, J. C., Cox, D. P., & Smith, B. W. 1976, ApJ, 204, 290

Snowden, S., Plucinsky, P., Briel, U., Hasinger, G., & Pfefferman, E. 1992, ApJ, 393, 819

Snowden, S., Burrows, D., & Mendenhall, J. 1994, ApJ, 999, 999

Stark, A. A., Gammie, C. F., Wilson, R. W., Bally, J., Linke, R. A., Heiles, C., & Hurwitz, M. 1992, ApJS, 79, 77

White, D. A., Fabian, A. C., Johnstone, R. M., Mushotzky, R. F., & Arnaud, K. A. 1991, MNRAS, 252, 72
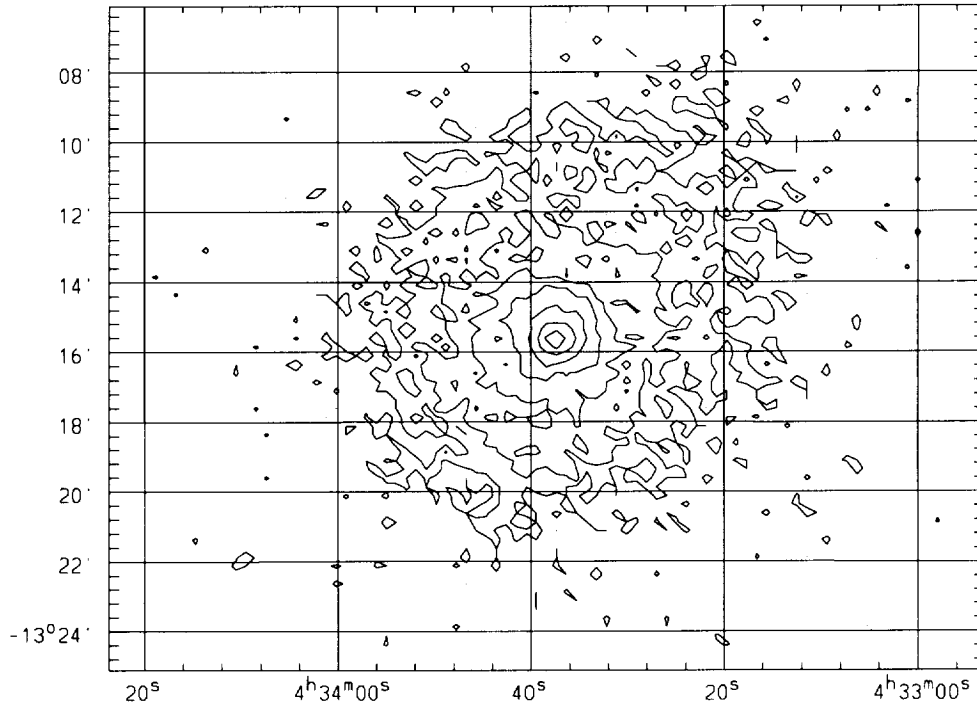
Fig. 1.— Contour plot of the vignetting-corrected ROSAT image of A 496. The image has been blocked into pixels of 15″. Contour levels are set at 5, 10, 20, 40, 80, 140, and 220 counts per pixel.
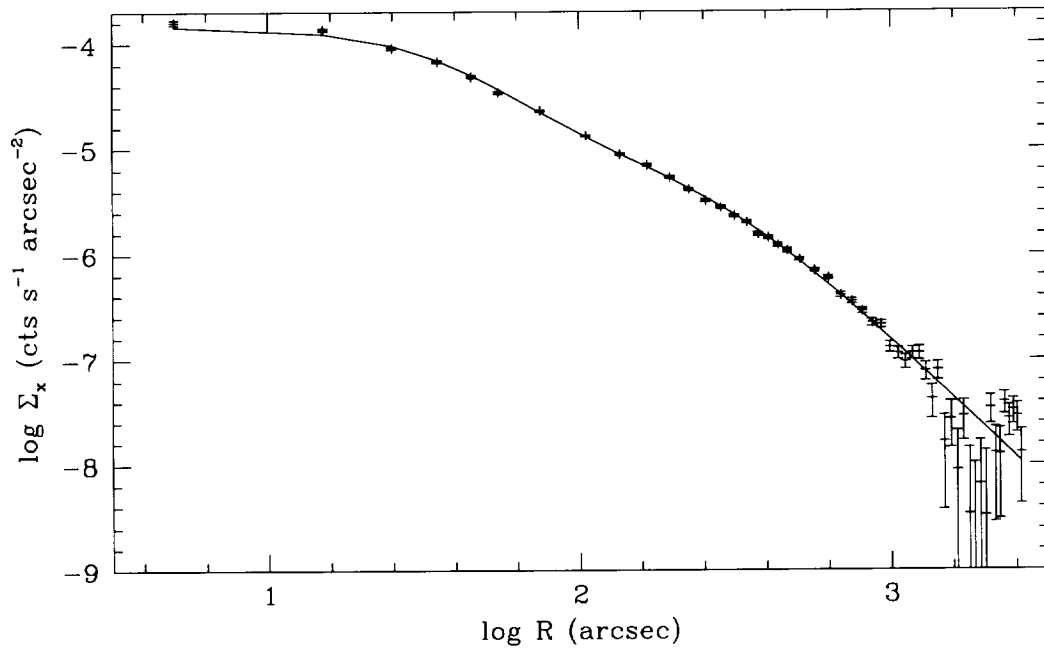
Fig. 2.— The X-ray surface brightness profile of A 496 as seen with the ROSAT PSPC. The scale on the sky is $0\farcs91$ kpc per arcsec. A uniform background of 3.4×10^{-7} cts s^{-1} arcsec^{-2} has been subtracted from the vignetting-corrected image. Error bars are 1σ statistical errors. The thin solid line is the best-fit, two component β-model.
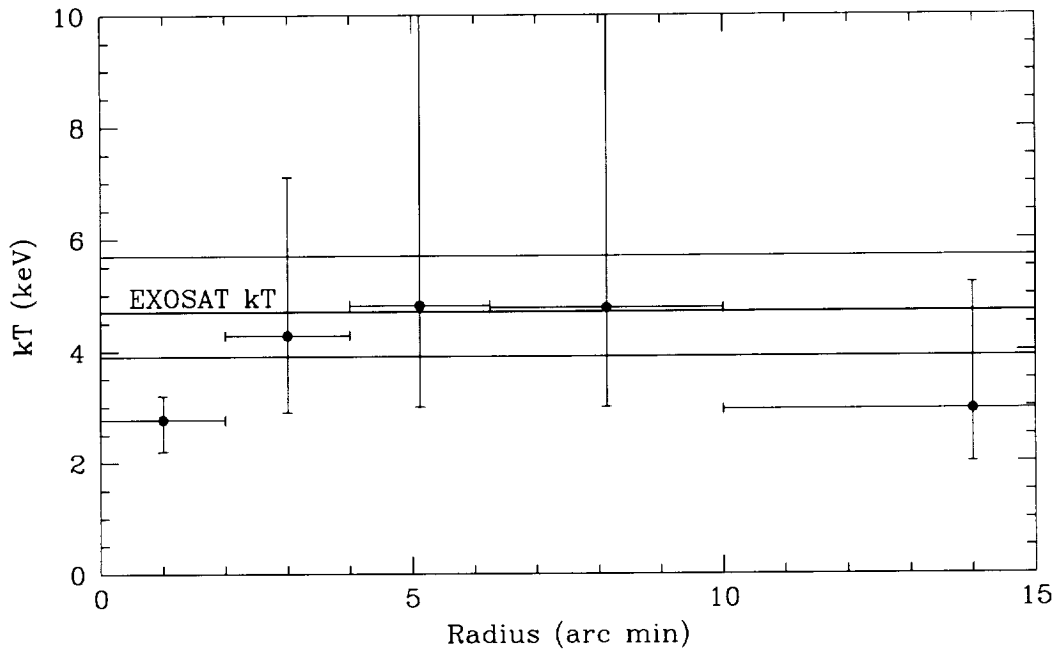
Fig. 3.— The temperature gradient indicative of a cooling flow is shown in this plot of the best-fit temperature *vs.* radius in A 496. Error bars are 90% confidence for two interesting parameters. The heavy solid line is the best-fit temperature from the medium energy EXOSAT observations of Edge & Stewart (1991). The lighter solid lines to either side are the 90% confidence limits on their temperature determination.
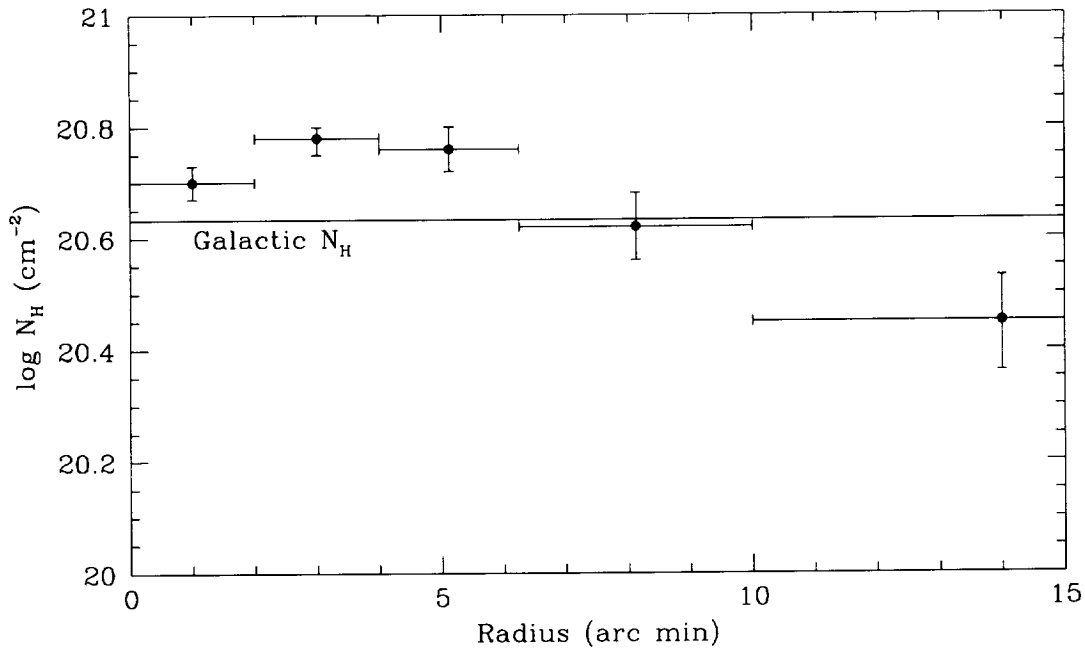
Fig. 4.— The spatial variation of the low energy absorption in A 496 is illustrated in this plot of log N_H vs. radius. Error bars are 90% confidence for two interesting parameters. The solid line illustrates the galactic column density along this sight line from Stark et al. (1992).
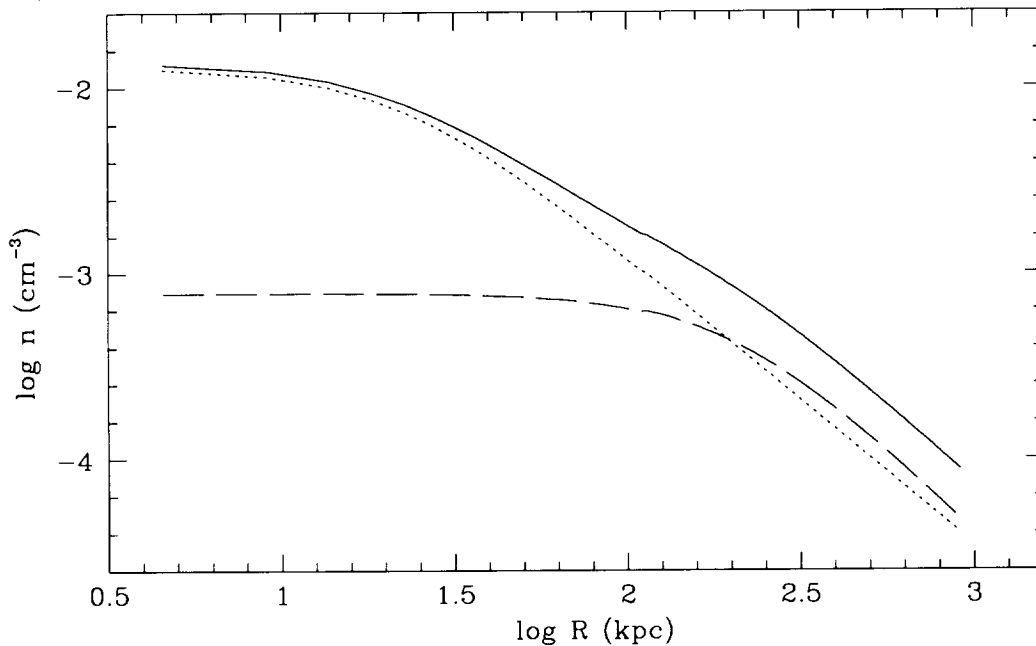

Fig. 5.— The density of the X-ray emitting gas in A 496 as derived from the fitted X-ray surface brightness profile. The total density is shown as a solid line. The component associated with the small core-radius portion of the two-component β-model is shown as a dotted line. The large core-radius, cluster-filling component is shown as a dotted line.
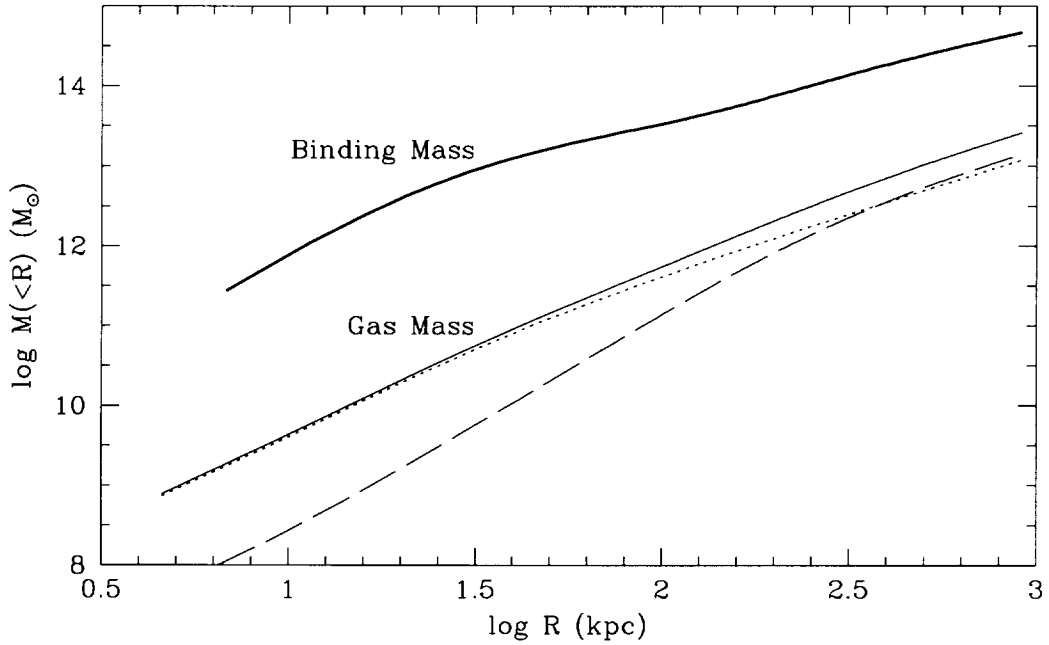
Fig. 6.— The integral mass distribution of the X-ray emitting gas in A 496 is shown as a thin solid line. The mass associated with the small core-radius portion of the two-component β-model is shown as a dotted line. The large core-radius, cluster-filling component is shown as a dotted line. The total integral mass distribution of the cluster, including unseen binding mass, is shown as a heavy solid line.